First-Principles Modelling of Heterogeneous Electrochemical Reactions

Celebrating the Life of Suning Wang—CCCE 2021

Leanne D. Chen

August 16th, 2021

Department of Chemistry

UNIVERSITY of GUELPH

ELECTROCHEMICAL TECHNOLOGY CENTRE
DEPARTMENT OF CHEMISTRY

The Climate Challenge

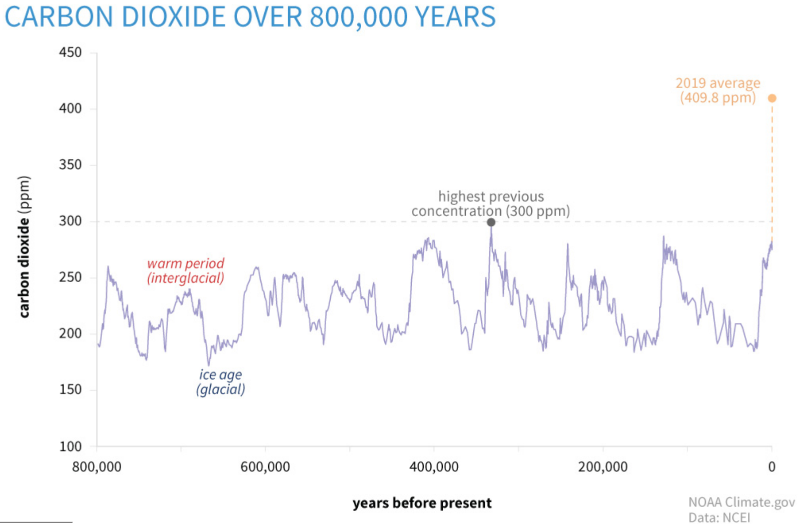

Levelized Cost of Energy Comparison

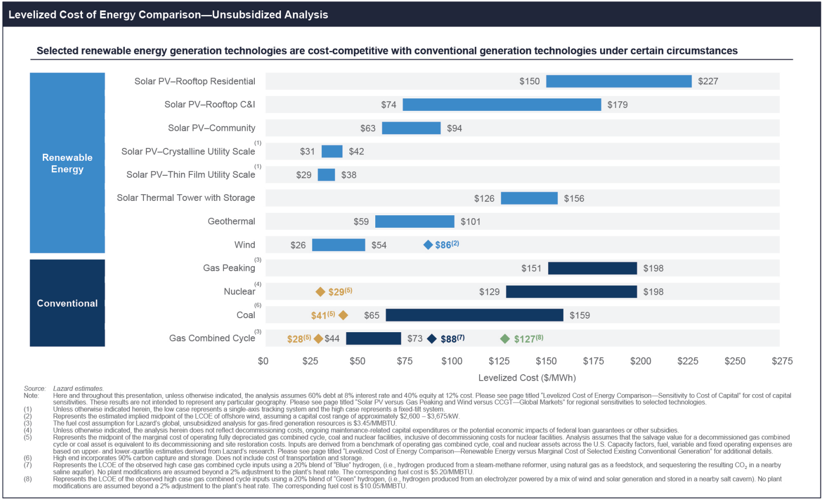

Levelized Cost of Energy Comparison—Unsubsidized Analysis

Selected renewable energy generation technologies are cost-competitive with conventional generation technologies under certain circumstances

Source: *Lazard estimates.*

Note: Here and throughout this presentation, unless otherwise indicated, the analysis assumes 60% debt at 8% interest rate and 40% equity at 12% cost. Please see page titled "Levelized Cost of Energy Comparison—Sensitivity to Cost of Capital" for cost of capital sensitivities. These results are not intended to represent any particular geography. Please see page titled "Solar PV versus Gas Peaking and Wind versus CCGT—Global Markets" for regional sensitivities to selected technologies.

(1) Unless otherwise indicated herein, the low case represents a single-axis tracking system and the high case represents a fixed-tilt system.

(2) Represents the estimated implied midpoint of the LCOE of offshore wind, assuming a capital cost range of approximately $2,600 – $3,675/kW.

(3) The fuel cost assumption for Lazard's global, unsubsidized analysis for gas-fired generation resources is $3.45/MMBTU.

(4) Unless otherwise indicated, the analysis herein does not reflect decommissioning costs, ongoing maintenance-related capital expenditures or the potential economic impacts of federal loan guarantees or other subsidies.

(5) Represents the midpoint of the marginal cost of operating fully depreciated gas combined cycle, coal and nuclear facilities, inclusive of decommissioning costs for nuclear facilities. Analysis assumes that the salvage value for a decommissioned gas combined cycle or coal asset is equivalent to its decommissioning and site restoration costs. Inputs are derived from a benchmark of operating gas combined cycle, coal and nuclear assets across the U.S. Capacity factors, fuel, variable and fixed operating expenses are based on upper- and lower-quartile estimates derived from Lazard's research. Please see page titled "Levelized Cost of Energy Comparison—Renewable Energy versus Marginal Cost of Selected Existing Conventional Generation" for additional details.

(6) High end incorporates 90% carbon capture and storage. Does not include cost of transportation and storage.

(7) Represents the LCOE of the observed high case gas combined cycle inputs using a 20% blend of "Blue" hydrogen, (i.e., hydrogen produced from a steam-methane reformer, using natural gas as a feedstock, and sequestering the resulting CO_2 in a nearby saline aquifer). No plant modifications are assumed beyond a 2% adjustment to the plant's heat rate. The corresponding fuel cost is $5.20/MMBTU.

(8) Represents the LCOE of the observed high case gas combined cycle inputs using a 20% blend of "Green" hydrogen, (i.e., hydrogen produced from an electrolyzer powered by a mix of wind and solar generation and stored in a nearby salt cavern). No plant modifications are assumed beyond a 2% adjustment to the plant's heat rate. The corresponding fuel cost is $10.05/MMBTU.

The Energy Transformation Challenge

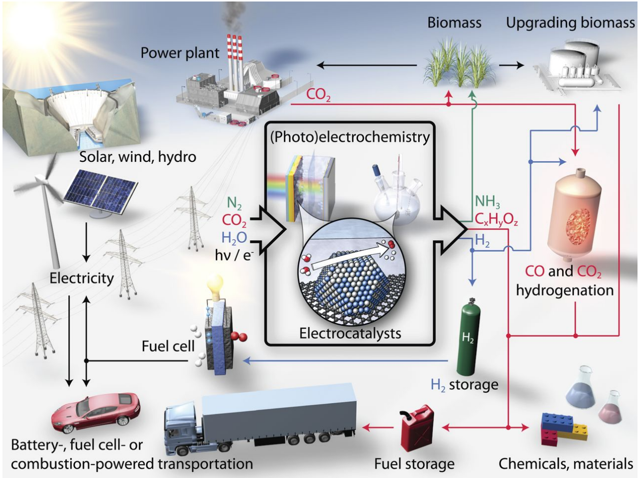

Seh, Z. W.; Kibsgaard, J.; Dickens, C. F.; Chorkendorff, I.; Jaramillo, T. F. *Science* **2017**, *355*, eaad4998.

mechanistic understanding

↓

stable, active, and selective electrocatalysts

Improving Electrocatalytic Activity

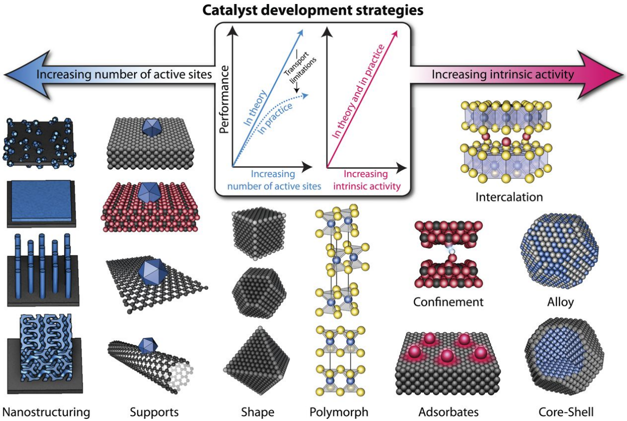

Seh, Z. W.; Kibsgaard, J.; Dickens, C. F.; Chorkendorff, I.; Jaramillo, T. F. *Science* **2017**, *355*, eaad4998.

mechanistic understanding

↓

stable, active, and selective electrocatalysts

Theory + Experiment

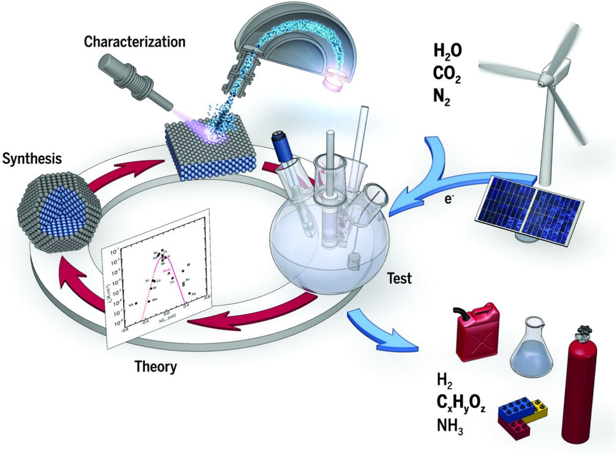

mechanistic understanding

↓

stable, active, and selective electrocatalysts

Seh, Z. W.; Kibsgaard, J.; Dickens, C. F.; Chorkendorff, I.; Jaramillo, T. F. *Science* **2017**, *355*, eaad4998.

Surface Processes

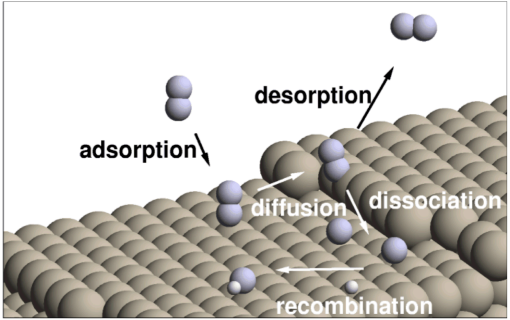

Figure 2.4 Illustration of the elementary reaction steps on surfaces.

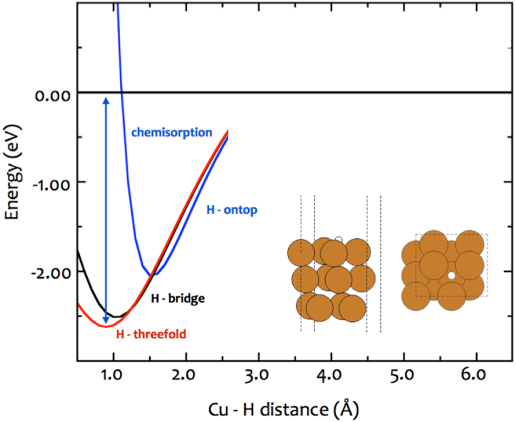

Nørskov, J. K.; Studt, F.; Abild-Pedersen, F.; Bligaard, T. John Wiley & Sons, Inc: Hoboken, NJ, USA, 2014.

Heterogeneous Electrocatalysis

Complexity:

- support
- electrode
- solvent
- dissolved species

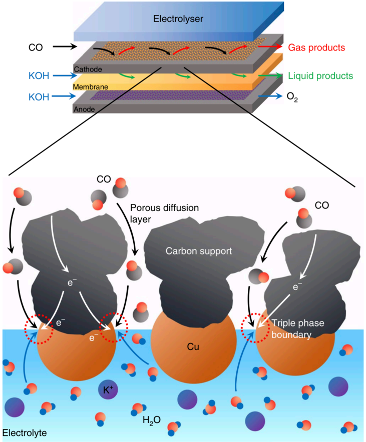

Jouny, M.; Luc, W.; Jiao, F. *Nat. Catal.* **2018**, *1*, 748–755.

Limiting Potential in the Al-Air Battery

Li-Ion versus Metal-Air Batteries

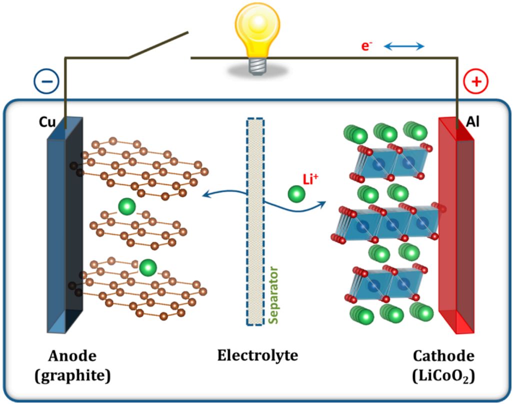

Goodenough, J. B.; Park, K.-S. *J. Am. Chem. Soc.* **2013**, *135*, 1167–1176.

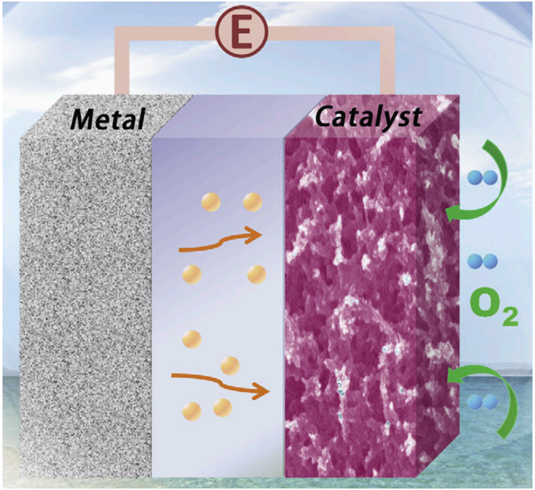

Cheng, F.; Chen, *J. Chem. Soc. Rev.* **2012**, *41*, 2172–2192.

Half-Reactions

Cathodic:

$$\frac{1}{2}\,\mathrm{O_2(g)} + \mathrm{H_2O(l)} + 2\,\mathrm{e^-} \rightarrow 2\,\mathrm{OH^-(aq)}, \quad U^{\ominus} = 0.4\ \text{V versus SHE} \tag{1}$$

Anodic:

$$\mathrm{Al(s)} + 3\,\mathrm{OH^-(aq)} \rightarrow \mathrm{Al(OH)_3(s)} + 3\,\mathrm{e^-}, \quad U^{\ominus} = -2.30\ \text{V versus SHE} \tag{2}$$

Theoretical cell voltage: 2.70 V

Practical anode voltage: −1.5 to −1.9 V[1]

[1] Egan, D. R.; Ponce de León, C.; Wood, R. J. K.; Jones, R. L.; Stokes, K. R.; Walsh, F. C. *J. Power Sources* **2013**, *236*, 293–310.

Stepwise Mechanism

$$\textbf{Overall: } \mathrm{Al} + 3\ \mathrm{OH}^- \rightarrow \mathrm{Al(OH)_3(s)} + 3\ \mathrm{e}^- \tag{3}$$

$$\mathrm{Al} + \mathrm{OH}^-\mathrm{(aq)} \rightarrow \mathrm{AlOH}\ast + \mathrm{e}^- \tag{4}$$

$$\mathrm{AlOH}\ast + \mathrm{OH}^-\mathrm{(aq)} \rightarrow \mathrm{Al(OH)_2}\ast + \mathrm{e}^- \tag{5}$$

$$\mathrm{Al(OH)_2}\ast + \mathrm{OH}^-\mathrm{(aq)} \rightarrow \mathrm{Al(OH)_3}\ast + \mathrm{e}^- \tag{6}$$

$$\mathrm{Al(OH)_3}\ast \rightarrow \mathrm{Al(OH)_3(s)} \tag{7}$$

Macdonald, D. D. *J. Electrochem. Soc.* **1988**, *135*, 2410.

The Computational Hydrogen Electrode (CHE)

Our reference is the half-reaction

$$H^+(aq) + e^- \rightleftharpoons \frac{1}{2} H_2(g) \tag{8}$$

This reaction is defined to be at equilibrium at $U = 0$ V, pH $= 0$, and $p_{H_2} = 101325$ Pa. Then we can equate the chemical potentials of the proton-electron pair with half that of the gas-phase H_2 molecule

$$\mu_{H^+(aq)} + \mu_{e^-} = \frac{1}{2}\mu_{H_2(g)} \tag{9}$$

Additional terms are added to include the effects of pH and potential shifts

$$\mu_{H^+(aq)}([H^+]) + \mu_{e^-}(U) = \frac{1}{2}\mu_{H_2(g)} + RT\ln\left(\frac{\sqrt{p_{H_2}}}{[H^+]}\right) - eU \tag{10}$$

Nørskov, J.K.; Rossmeisl, J.; Logadottir, A.; Lindqvist, L.; Kitchin, J. R.; Bligaard, T.; Jónsson, H. *J. Phys. Chem. B* **2004**, *108*, 17886–17892.

The Computational Hydrogen Electrode (CHE)

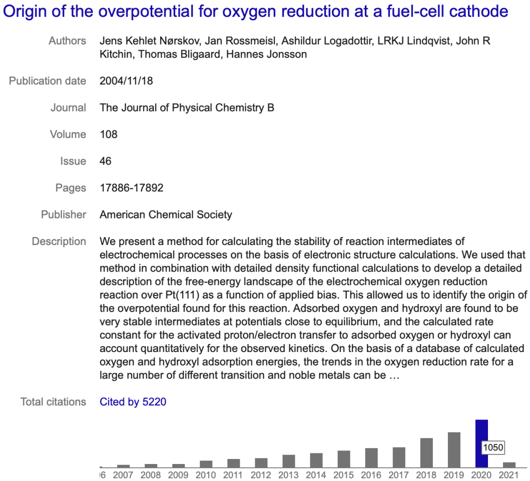

Origin of the overpotential for oxygen reduction at a fuel-cell cathode

Authors	Jens Kehlet Nørskov, Jan Rossmeisl, Ashildur Logadottir, LRKJ Lindqvist, John R Kitchin, Thomas Bligaard, Hannes Jonsson
Publication date	2004/11/18
Journal	The Journal of Physical Chemistry B
Volume	108
Issue	46
Pages	17886-17892
Publisher	American Chemical Society
Description	We present a method for calculating the stability of reaction intermediates of electrochemical processes on the basis of electronic structure calculations. We used that method in combination with detailed density functional calculations to develop a detailed description of the free-energy landscape of the electrochemical oxygen reduction reaction over Pt(111) as a function of applied bias. This allowed us to identify the origin of the overpotential found for this reaction. Adsorbed oxygen and hydroxyl are found to be very stable intermediates at potentials close to equilibrium, and the calculated rate constant for the activated proton/electron transfer to adsorbed oxygen or hydroxyl can account quantitatively for the observed kinetics. On the basis of a database of calculated oxygen and hydroxyl adsorption energies, the trends in the oxygen reduction rate for a large number of different transition and noble metals can be …
Total citations	Cited by 5220

Applying the CHE

$$\mathrm{H_2O(l)} + \mathrm{e^-} \rightleftharpoons \frac{1}{2}\,\mathrm{H_2(g)} + \mathrm{OH^-(aq)}, \quad U^{\ominus} = -0.83\ \mathrm{V\ versus\ SHE,\ pH} = 14 \tag{11}$$

$$\mu_{\mathrm{OH^-(aq)}} - \mu_{\mathrm{e^-}} = \mu_{\mathrm{H_2O(l)}} - \frac{1}{2}\mu_{\mathrm{H_2(g)}} + RT\ln\left(\frac{\sqrt{p_{\mathrm{H_2}}}\,[\mathrm{OH^-}]}{a_{\mathrm{H_2O(l)}}}\right) - (0.83 + eU) \tag{12}$$

To calculate the energy of the first adsorption step

$$\mathrm{Al} + \mathrm{OH^-(aq)} \rightarrow \mathrm{AlOH}\star + \mathrm{e^-} \tag{13}$$

We have

$$\Delta G = G_{\mathrm{AlOH}\star} - G_{\mathrm{Al}} - \left[\mu_{\mathrm{H_2O(l)}} - \frac{1}{2}\mu_{\ \mathrm{H_2(g)}} + RT\ln\left(\frac{\sqrt{p_{\mathrm{H_2}}}\,[\mathrm{OH^-}]}{a_{\mathrm{H_2O(l)}}}\right) - (0.83 + eU)\right] \tag{14}$$

Chen, L. D.; Luntz, A. C.; Nørskov, J. K. *J. Phys. Chem. Lett.* **2014**, *119*, 19660–19667.

Reaction Energetics on the Close-Packed Al(111) Surface

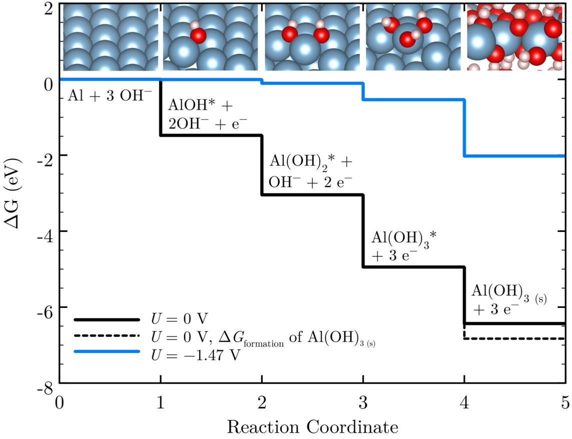

Chen, L. D.; Luntz, A. C.; Nørskov, J. K. *J. Phys. Chem. Lett.* **2014**, *119*, 19660–19667.

Black: 0 V versus SHE

Blue: −1.47 V versus SHE, limiting potential on this facet

Practical anode voltages: −1.5 to −1.9 V[1]

[1] Egan, D. R.; Ponce de León, C.; Wood, R. J. K.; Jones, R. L.; Stokes, K. R.; Walsh, F. C. *J. Power Sources* **2013**, *236*, 293–310.

Reaction Energetics on the Stepped Al(211) Surface

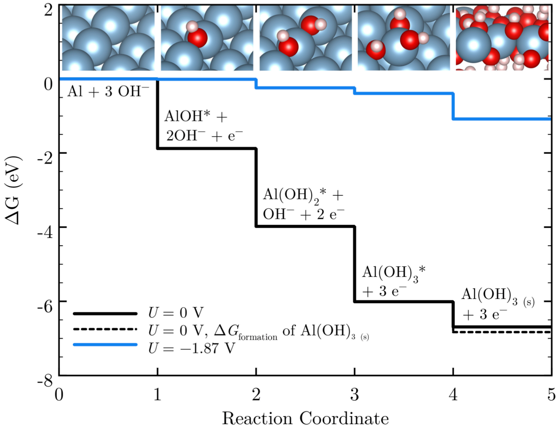

Chen, L. D.; Luntz, A. C.; Nørskov, J. K. *J. Phys. Chem. Lett.* **2014**, *119*, 19660–19667.

Black: 0 V versus SHE

Blue: −1.87 V versus SHE, limiting potential on this facet

Practical anode voltages: −1.5 to −1.9 V[1]

[1] Egan, D. R.; Ponce de León, C.; Wood, R. J. K.; Jones, R. L.; Stokes, K. R.; Walsh, F. C. *J. Power Sources* **2013**, *236*, 293–310.

UNIVERSITY of GUELPH

Factors Contributing to the Overpotential

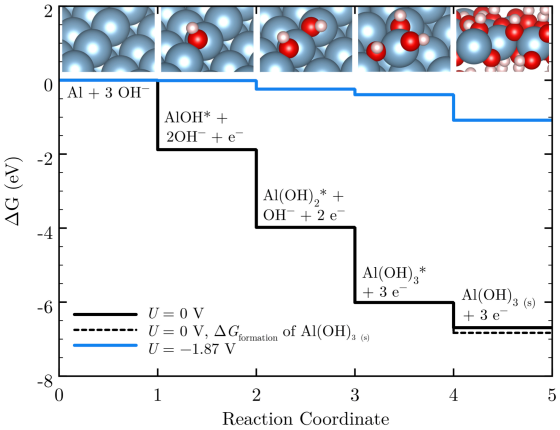

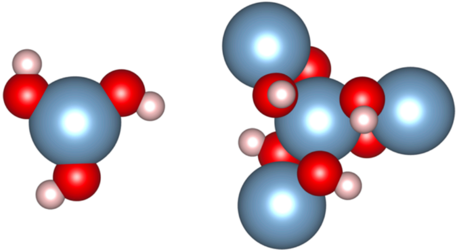

Surface and bulk $Al(OH)_3$

Chen, L. D.; Luntz, A. C.; Nørskov, J. K. *J. Phys. Chem. Lett.* **2014**, *119*, 19660–19667.

Voltage Limitations Are Intrinsic to the Anode

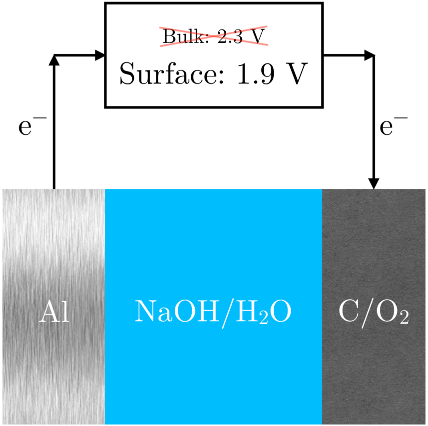

Chen, L. D.; Luntz, A. C.; Nørskov, J. K. *J. Phys. Chem. Lett.* **2014**, *119*, 19660–19667.

UNIVERSITY of GUELPH

Field Effects in CO_2 Reduction

CO_2 Reduction Activity and Selectivity Challenges

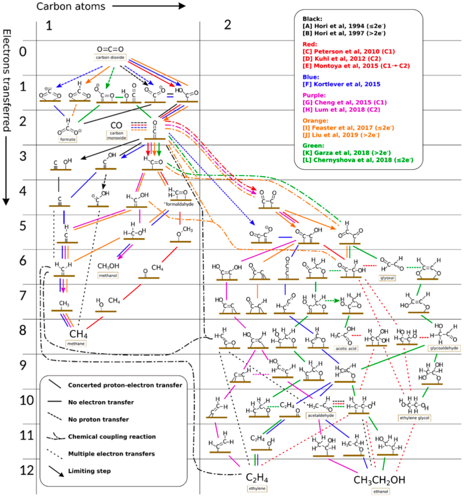

Nitopi, S. et al. *Chem. Rev.* **2019**, *119*, 7610–7672.

Cation Effects

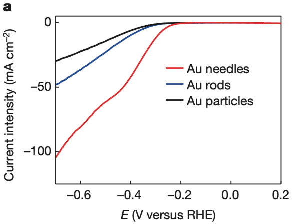

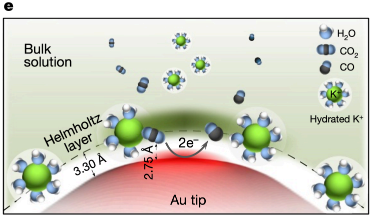

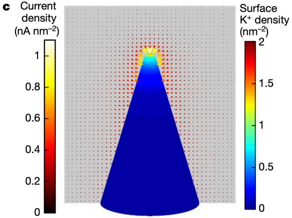

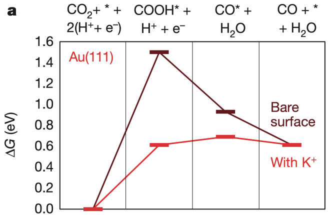

Liu, M.; Pang, Y.; Zhang, B.; De Luna, P.; Voznyy, O.; Xu, J.; Zheng, X.; Dinh, C. T.; Fan, F.; Cao, C.; García de Arquer, F. P.; Safaei, T. S.; Mepham, A.; Klinkova, A.; Kumacheva, E.; Filleter, T.; Sinton, D.; Kelley, S. O.; Sargent, E. H. *Nature* **2016**, *537*, 382–386.

Stepwise Mechanism for CO_2 Reduction to CO

Overall:

$$CO_2(g) + H_2O(l) + 2\ e^- \rightarrow CO(g) + 2\ OH^-(aq) \tag{15}$$

$$CO_2(g) + * \rightarrow *CO_2 \tag{16}$$

$$*CO_2 + H_2O(l) + e^- \rightarrow *COOH + OH^-(aq) \tag{17}$$

$$*COOH + e^- \rightarrow *CO + OH^-(aq) \tag{18}$$

$$*CO \rightarrow CO(g) \tag{19}$$

Using the CHE Model for CO_2 Reduction to CO

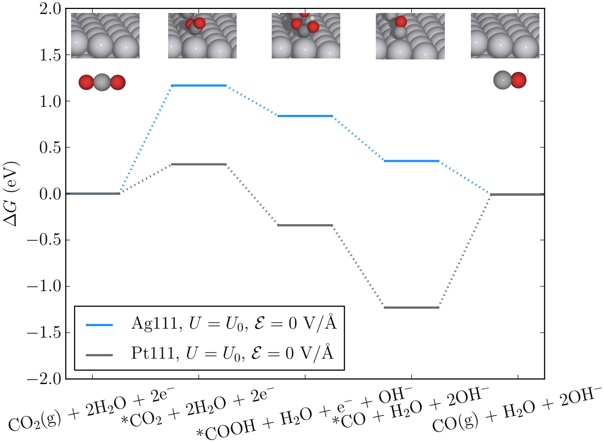

Threshold for facile kinetics:

0.75 eV (1 reaction site^{-1} s^{-1})

Chen, L. D.; Urushihara, M.; Chan, K.; Nørskov, J. K. *ACS Catal.* **2016**, *6*, 7133–7139.

Stabilization of $*CO_2$

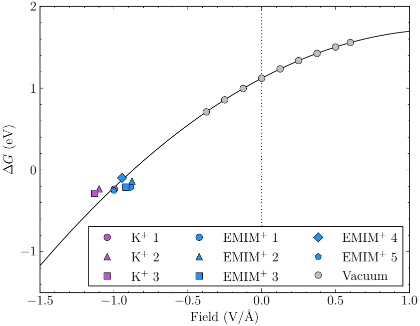

Chen, L. D.; Urushihara, M.; Chan, K.; Nørskov, J. K. *ACS Catal.* **2016**, *6*, 7133–7139.

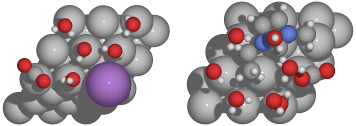

$$V_{\text{effective}} = V_{\text{env}} - V_{\text{slab}} - V_{\text{solvent}} - V_{\text{ion}} \qquad (20)$$

$$\varepsilon = -\left(-\frac{dV}{dz}\right) \qquad (21)$$

Energy Diagram Comparison

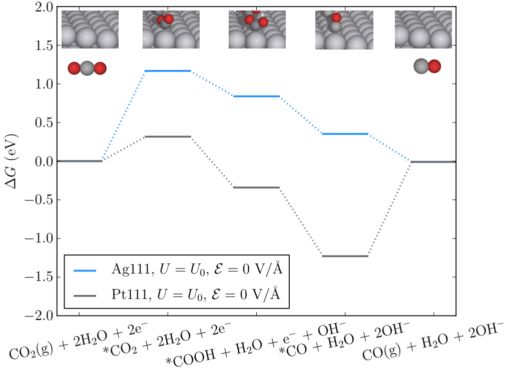

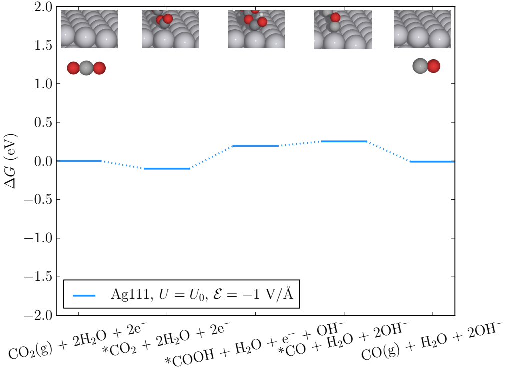

Electric Field Is Not Uniform

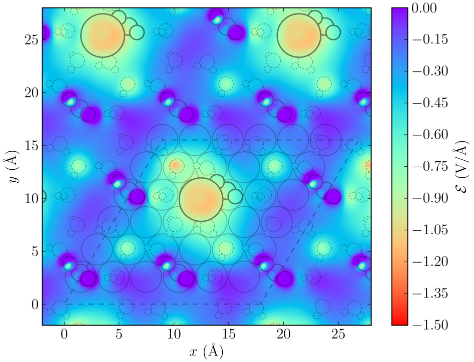

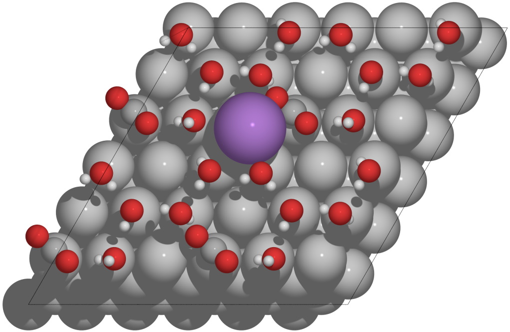

Chen, L. D.; Urushihara, M.; Chan, K.; Nørskov, J. K. *ACS Catal.* **2016**, *6*, 7133–7139.

Microkinetic Modelling

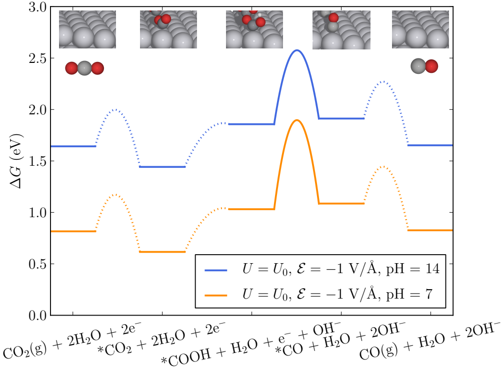

$$r_1 = k_{1\blacktriangleright} p_{CO_2} \theta_* - k_{1\blacktriangleleft} \theta_{CO_2} \tag{22}$$

$$r_2 = k_{2\blacktriangleright} \theta_{CO_2} - k_{2\blacktriangleleft} \left[OH^-\right] \theta_{COOH} \tag{23}$$

$$r_3 = k_{3\blacktriangleright} \theta_{COOH} - k_{3\blacktriangleleft} \left[OH^-\right] \theta_{CO} \tag{24}$$

$$r_4 = k_{4\blacktriangleright} \theta_{CO} - k_{4\blacktriangleleft} p_{CO} \theta_* \tag{25}$$

Microkinetic Modelling

$$k_i = \frac{k_\mathrm{B} T}{h} \exp\left(-\frac{E^{\ominus}_{\mathrm{a},i}}{k_\mathrm{B} T}\right) \exp\left[-\frac{e\beta_i\left(U - U^{\ominus}_i\right)}{k_\mathrm{B} T}\right] \tag{26}$$

$$K_i = \exp\left(-\frac{\Delta G_i}{k_\mathrm{B} T}\right) \tag{27}$$

$$\begin{aligned} r_\text{field} = {} & k_{3\blacktriangleright} \frac{K_{1\blacktriangleright} K_{2\blacktriangleright} p_{\mathrm{CO_2}}}{\left[\mathrm{OH^-}\right]} \frac{1}{1 + K_{1\blacktriangleright} p_{\mathrm{CO_2}} + K_{1\blacktriangleright} K_{2\blacktriangleright} p_{\mathrm{CO_2}} / \left[\mathrm{OH^-}\right] + K_{4\blacktriangleleft} p_\mathrm{CO}} \\ & - k_{3\blacktriangleleft} \left[\mathrm{OH^-}\right] K_{4\blacktriangleleft} p_\mathrm{CO} \frac{1}{1 + K_{1\blacktriangleright} p_{\mathrm{CO_2}} + K_{1\blacktriangleright} K_{2\blacktriangleright} p_{\mathrm{CO_2}} / \left[\mathrm{OH^-}\right] + K_{4\blacktriangleleft} p_\mathrm{CO}} \end{aligned} \tag{28}$$

Comparing Computed Rates to Experiment

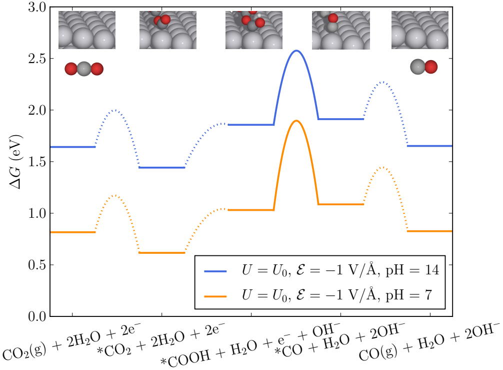

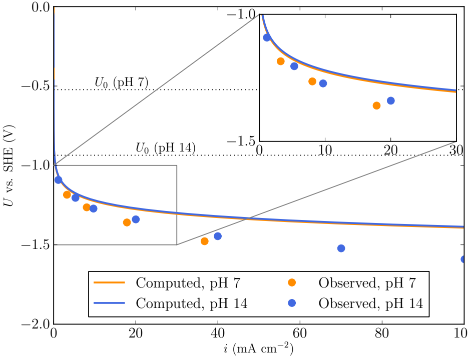

Chen, L. D.; Urushihara, M.; Chan, K.; Nørskov, J. K. *ACS Catal.* **2016**, *6*, 7133–7139 with data adapted from Thorson, M. R.; Siil, K. I.; Kenis, P. J. A. *J. Electrochem. Soc.* **2013**, *160*, F69–F74.

Fractional Charge of Interfacial Ions

Volmer Reaction Energies

CHE:

$$\mathrm{H^+(bulk\ solution)} + \mathrm{e^-} + * \rightarrow \mathrm{H}*$$
$$\Delta G = \Delta G^{\ominus} + eU \qquad (29)$$

Explicit Solvent:

$$\mathrm{H^+(double\ layer)} + \mathrm{e^-} + * \rightarrow \mathrm{H}*$$
$$\Delta G = \Delta G^{\ominus} + 0.66eU \qquad (30)$$

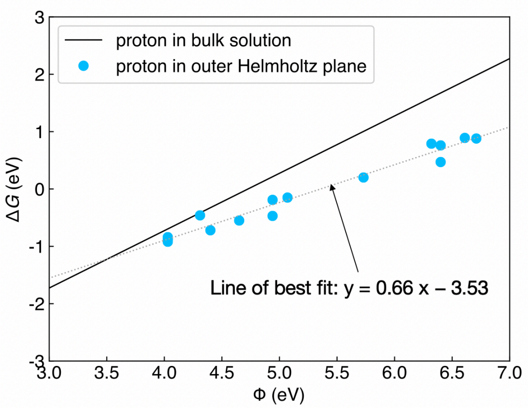

UNIVERSITY of GUELPH

Possible Sources of Error

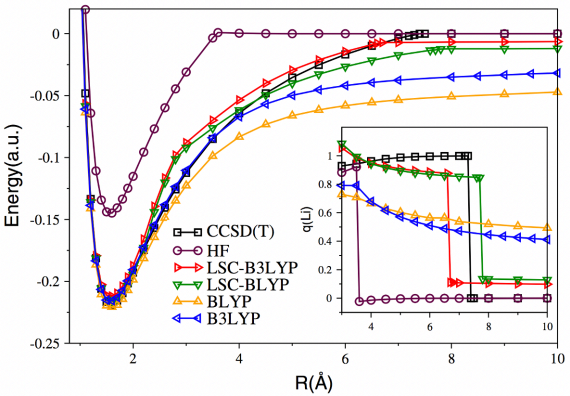

Li, C.; Zheng, X.; Cohen, A. J.; Mori-Sánchez, P.; Yang, W. *Phys. Rev. Lett.* **2015**, *114*, 053001.

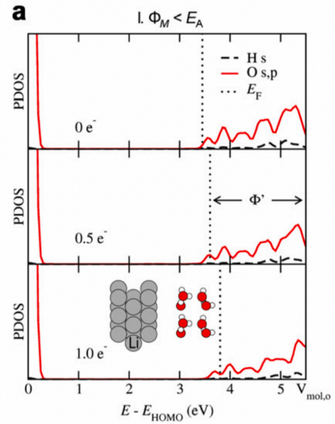

Björketun, M. E.; Zeng, Z.; Ahmed, R.; Tripković, V.; Thygesen, K. S.; Rossmeisl, J. *Chem. Phys. Lett.* **2013**, *555*, 145–148.

Simulation System

Top: proton solvated in the first solvent layer (outer Helmholtz plane)

Bottom: proton solvated in the third solvent layer (bulk solution)

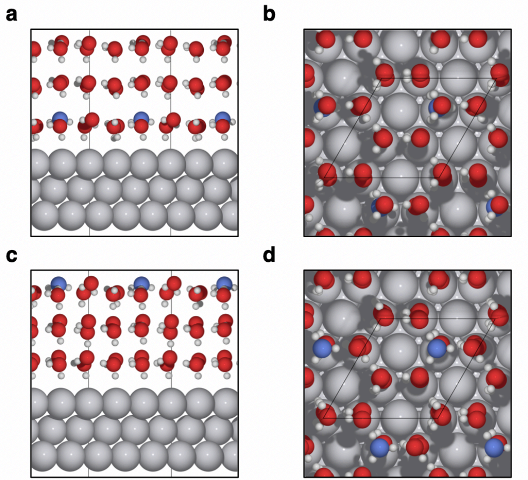

Comparing Different Functionals

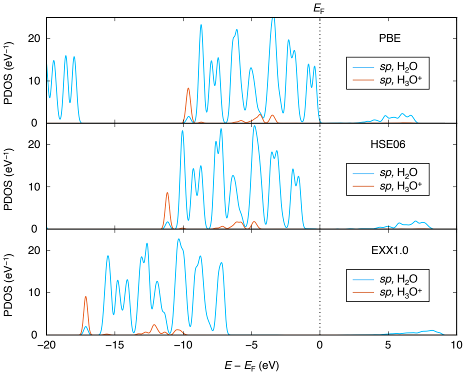

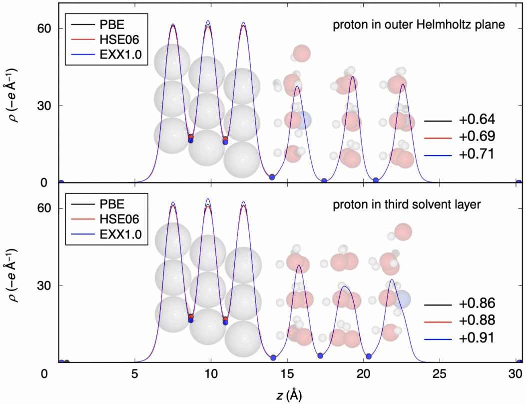

Chen, L. D.; Bajdich, M.; Martirez, J. M. P.; Krauter, C. M.; Gauthier, J. A.; Carter, E. A.; Luntz, A. C.; Chan, K.; Nørskov, J. K. *Nat. Commun.* **2018**, *9*, 3202.

Embedded Calculations

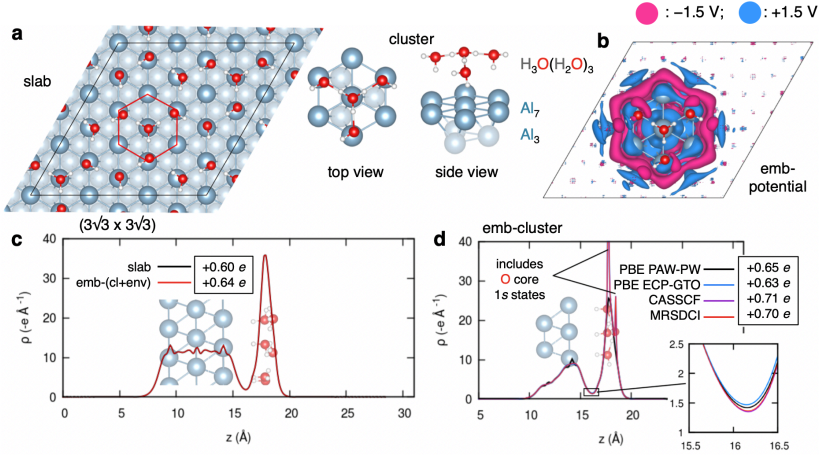

Chen, L. D.; Bajdich, M.; Martirez, J. M. P.; Krauter, C. M.; Gauthier, J. A.; Carter, E. A.; Luntz, A. C.; Chan, K.; Nørskov, J. K. *Nat. Commun.* **2018**, *9*, 3202.

Fractional Charge Not Due to Delocalization or Band Misalignment

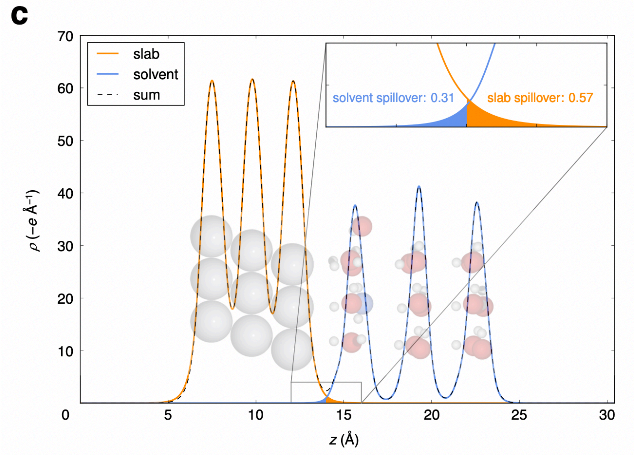

Chen, L. D.; Bajdich, M.; Martirez, J. M. P.; Krauter, C. M.; Gauthier, J. A.; Carter, E. A.; Luntz, A. C.; Chan, K.; Nørskov, J. K. *Nat. Commun.* **2018**, *9*, 3202.

Looking Ahead

Current Work

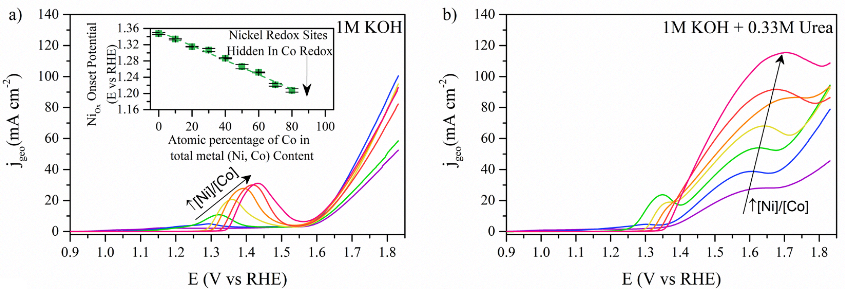

Stephen W. Tatarchuk

Rachelle M. Choueiri

Anna Klinkova

Tatarchuk, S. W.; Choueiri, R. M.; Medvedev, J.; Chen, L. D.; Klinkova, A. *Chemosphere* **2021**, *279*, 130550.

Current Work

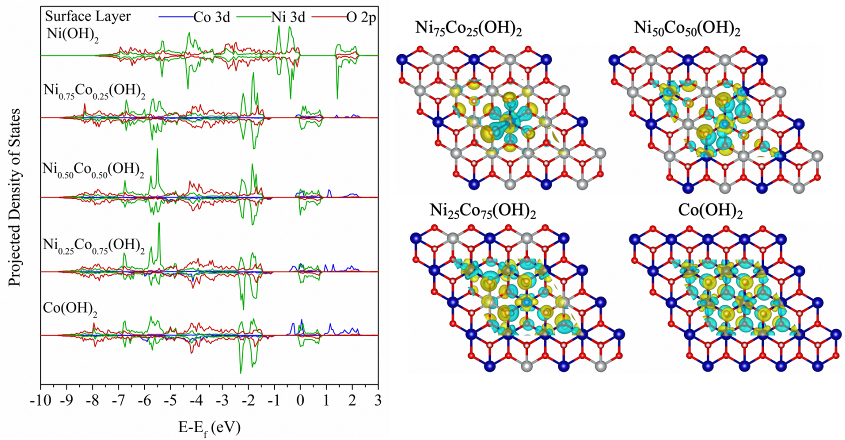

Tatarchuk, S. W.; Choueiri, R. M.; Medvedev, J.; Chen, L. D.; Klinkova, A. *Chemosphere* **2021**, *279*, 130550.

Current Work

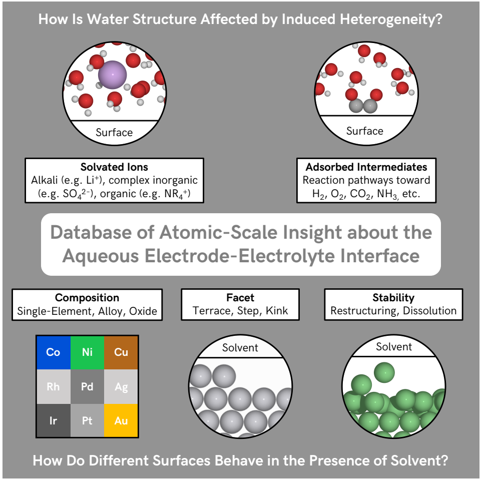

How Is Water Structure Affected by Induced Heterogeneity?

Solvated Ions
Alkali (e.g. Li$^+$), complex inorganic (e.g. SO_4^{2-}), organic (e.g. NR_4^+)

Adsorbed Intermediates
Reaction pathways toward H_2, O_2, CO_2, NH_3, etc.

Database of Atomic-Scale Insight about the Aqueous Electrode-Electrolyte Interface

Composition
Single-Element, Alloy, Oxide

Facet
Terrace, Step, Kink

Stability
Restructuring, Dissolution

Co	Ni	Cu
Rh	Pd	Ag
Ir	Pt	Au

How Do Different Surfaces Behave in the Presence of Solvent?

Acknowledgements


Jens Nørskov (L) and Alan Luntz (R)


Karen Chan

Collaborators:

- M. Urushihara
- E. A. Carter
- J. M. P. Martirez
- C. M. Krauter
- J. A. Gauthier
- M. Bajdich
- S. W. Tatarchuk
- R. M. Choueiri
- A. Klinkova

Acknowledgements

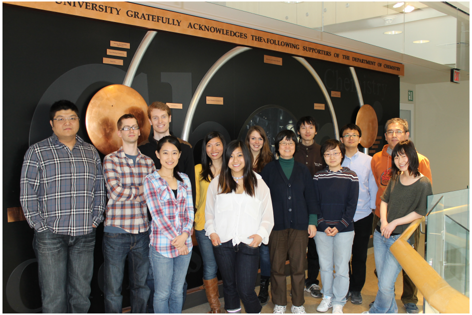

Thank you to the Conference Organizers, in particular Dr. Zachary Hudson and Dr. Barry Blight, for inviting me to this Symposium to celebrate the life of my former mentor, Dr. Suning Wang.